Journal of Nuclear Materials 105 (1982) 276–292
North-Holland Publishing Company

A RATE THEORY OF SWELLING INDUCED BY HELIUM AND DISPLACEMENT DAMAGE IN FUSION REACTOR STRUCTURAL MATERIALS

N.M. GHONIEM

School of Engineering and Applied Science, University of California at Los Angeles, California 90024, USA

and

M.L. TAKATA

EG&G, Idaho Falls, Idaho 83415, USA

Received 25 March 1981, accepted 26 October 1981

The combination of helium gas and displacement damage production in fusion reactor structural materials is detrimental to their integrity A simplified rate theory is presented to explain existing fission reactor swelling data The theory is applied also to fusion reactor conditions in both the steady-state and pulsed modes of operation In this time-dependent rate theory both the nucleation and growth phases of cavities are treated The smooth transition from nucleation to growth is achieved by developing an approximate equation for the time-dependent nucleation current. This current decreases sharply after the formation of the majority of cavities. Cavity growth then controls the overall swelling It is shown that the dynamic dispersion of helium atoms into the matrix by radiation (re-solution) plays an important role at low temperature Radiation pulsing of the tokamak-type results in a higher effective mobility for helium. This is attributed to the annealing of helium vacancy traps in between pulses Overall lower cavity concentrations are therefore expected in this particular situation.

1. Introduction and background

Fusion reactor first walls are expected to withstand severe operational environments. Aside from the detrimental effects of radiation damage, nuclear reactions produce both solid and gas transmutants in the structural materials. The generation of helium as a result of transmutation reactions arouses concern about its effects on the long-term integrity of the first wall. The presence of helium has been recognized to degrade the high temperature ductility of stainless steel [1]. Also, cavity formation and swelling of metals were shown to be strongly influenced by the presence of helium [2].

Helium is thermodynamically insoluble in metals and tends to precipitate into bubbles if the temperature is high enough for the helium atoms to migrate. Whereas helium concentrations in steel typical of fission reactor environments are in the range of 1–10 appm [3], the situation is expected to be more severe for Magnetic Confinement Fusion Reactors (MCFR's) because the transmutation cross sections for the 14 MeV neutrons are much higher. Generation rates are projected to be considerably greater than fast breeder reactors with up to 644 appm/yr in the Princeton design [4], 285 appm/yr in the Wisconsin design [5], and ~ 294 appm/yr for the INTOR design [6].

The helium content and the high ratio of helium concentration to displacement damage predicted for fusion reactors has given rise to the expectation that bubbles rather than voids may exist in fusion reactor structural materials [7,8]. The synergistic effects of helium and displacement damage have been experimentally shown to produce a significant influence on the microstructural evolution [9,10].

Choyke et al. [11] compared the effects of predoping versus coimplantation of helium in solution annealed 304 stainless steel bombarded with 28 MeV Si^{+6} at temperatures from 400 to 750°C. The helium concentration and implantation mode were observed to affect the ease of forming cavities, precipitates, and dislocation loops.

Wiffen and Bloom [12] irradiated stainless steel samples in the High Flux Isotope Reactor (HFIR) at temperatures of 380 to 680° with up to 120 displacements

0022-3115/82/0000–0000/$02.75

per atom (dpa) and helium concentrations up to 6090 ppm. Swelling in the solution annealed specimens was found to be smaller than predicted by equilibrium helium bubble swelling models but larger than the fast reactor irradiation results. Approximate gas balance calculations suggested that for irradiation at temperatures greater than 547°C the cavities were helium bubbles.

Hall's [13] time-dependent nucleation model described interstitial loop formation and growth, and vacancy clustering. The mobility of vancancies, self-interstitials, and interstitial helium was assumed. Loops and cavities were considered to capture vacancies and interstitials and emit vacancies. In addition, the spherical cavities were assumed to capture and emit helium gas atoms. The helium gas emission processes included thermal emission, displacement due to irradiation, and interstitial replacement. Odette and Frei [14] assumed that substitutional helium is continuously generated and that it diffuses until it encounters another helium to form a bubble nucleus or joins an existing bubble or void nucleus. Two sets of ordinary differential equations describe the bubble and void nucleus evolution coupled by bubble size dependent nucleation rates.

Maydet and Russel [15] developed a numerical simulation of void nucleation in irradiated metals in the presence of helium gas. A void is characterized by its vacancy content and the number of gas atoms it contains. Voids are assumed to capture vacancies, self-interstitials, and gas atoms and thermally emit vacancies and gas atoms. Only interstitial helium formed by radiation re-solutioning is assumed mobile. Li et al. [16] modified the GRASS code to examine helium behavior in stainless steel. The code was developed to model the formation and migration of fission gas bubbles in ceramic fuels. Gas bubbles can reside in the matrix, get trapped on dislocations and grain boundaries, or belong the grain edges. Bulk pores can grow by coalescence of cavities and vacancy absorption. Biased bubble motion due to a temperature gradient, re-solution of gas bubbles, and other features are suppressed The helium generation rate, the estimated helium bubble diffusivity, the dependence of diffusivity on bubble size, and grain size are included in the model. The bubble size distribution is determined by the simultaneous solution of a large set of coupled equations for bubbles. The bubbles are classified by an average size which is defined in terms of the number of gas atoms per bubble. A helium production rate of 500 appm/yr and a surface tension of 2000 ergs/cm^2 to balance the gas pressure were used in their calculation. A comparison of the results with HFIR's experimental data [12] indicated a significant difference of bulk bubble distributions and an agreement in the number density and size distributions of grain boundary cavities.

Theoretical modeling of the complex phenomena occurring in MCFR materials is necessary for explaining existing experiments and suggesting new ones. Fission reactors may not adequately simulate fusion conditions because the neutron energies are higher in a fusion reactor. Also, the neutron damage follows the burn and down cycles of the plasma in a fusion reactor, while it is essentially constant in a fission reactor. Fig. 1 shows the ranges of helium displacement damage accumulated in fusion reactor conceptual designs and simulation facilities after 1 year of irradiation. The data on fig. 1 is compiled mainly from ref. [3,6].

Type 316 stainless steel was selected as a representative first wall material in this study. Stainless steel is a good candidate for the first wall when considering swelling, embrittlement, yield strength, fracture toughness, creep strength, and compatibility with coolants and tritium; it is less favorable when accounting for surface

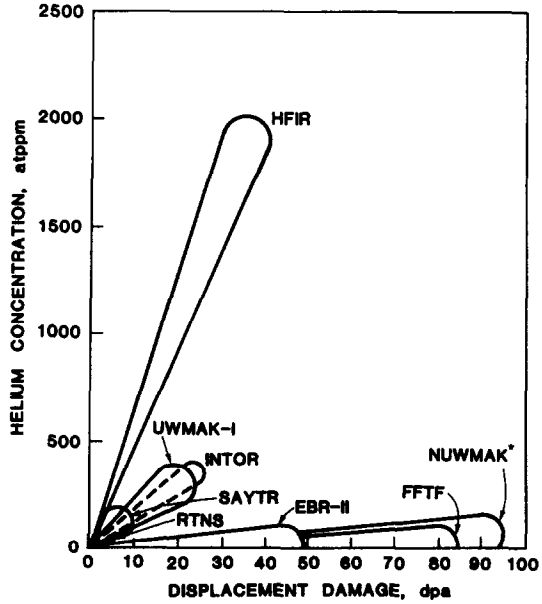

Fig 1. Helium concentration versus displacement damage in various fusion reactors in 316 stainless steel after 1 year of irradiation. INTOR ≡ International Tokamak Reactor [6], RTNS ≡ Rotating Target Neutron Source [3], EBR-II ≡ Experimental Breeder Reactor [3], FFTF ≡ Fast Flux Test Facility [3], SATYR ≡ UCLA conceptual design using a D–D fuel cycle and the mirror concept [45], UWMAK-I [5] and NUMAK [46] ≡ University of Wisconsin conceptual designs using a D–T fuel cycle and the Tokamak concept The first wall of NUWMAK is a Ti–6Al–4V alloy.

properties and thermal stress parameters [17].

In this paper, a mechanistic intragranular helium gas behavior model is developed for investigating the synergistic interaction of helium and displacement damage produced by neutron bombardment in fusion reactor structural materials. The model is based upon the homogeneous, time-dependent rate theory where conservation equations are used to describe the helium clusters and displacement damage components. In the next section, we discuss briefly helium migration mechanisms, and then follow this by an analysis of the process of helium dynamic re-solution by radiation in section 3. Section 4 outlines the theoretical and computational aspects of the present model. A comparison between the Helium Gas Behavior Under Fusion Conditions (HEGBUF) computer code results and the HFIR experimental data is presented in section 5. Applications of the model to various fusion designs are given in section 6, and the conclusions of the present work are presented in section 7.

2. Helium migration mechanisms

The migration mechanisms of helium in metals undergoing simultaneous radiation damage are not well established. Speculations for these mechanisms include substitutional, interstitial, mutual (interstitial + substitutional) diffusion, momentum transfer, diffusion by divacancies and various combinations of these mechanisms. It is not the intent of the present section to discuss the details and supporting evidence of all of these migration paths. However, selected theoretical and experimental evidence for helium migration by a trapping–detrapping mechanism will be briefly discussed

An interstitial migration mechanism was inferred from computer calculations of minimum energy lattice configurations for a variety of atomic jumps by helium atoms, vacancies, and self-interstitials in face-centered cubic metals [18]. There is strong evidence that helium has a low value for the activation energy for interstitial diffusion and a high interstitial formation energy [19]. Smidt and Pieper [20] found for stainless steel assuming 35 ppm He, a migration energy of 2.3 eV for the helium atom to reach a bubble. The value is close to the self-diffusion energy of nickel which is 2.8 to 2.9 eV. This was interpreted to be consistent with the motion of helium by a vacancy mechanism as a substitutional atom to form bubbles.

In a recent experimental investigation, Philipps et al. [21] conducted thermal desorption measurements in a thick nickel sample at temperatures between 900 and 1250°C. They established a migration energy of 0.8 eV for helium mobility under these non-irradiation conditions. The mechanism by which they interpreted their data is the helium trapping/detrapping in thermal vacancies.

Despite a strong technological need, helium migration in complex alloys has not yet been established [21a]. The problem in this area lies in the complicated paths by which helium can be transported in materials undergoing simultaneous radiation damage. Possible reactions for helium include:

(1) Trapping/detrapping in single vacancies, divacancies and higher order vacancy complexes.

(2) Trapping at dislocations and grain boundaries.

(3) Replacement of substitutional helium with self-interstitials.

(4) Clustering with other vacancies and helium.

(5) Re-solution from traps by irradiation.

(6) Migration as an interstitial, vacancy or in divacancies

In the present simplified theory, we will assume that the most abundant traps are the single vacancies, and that helium atoms migrate interstitially in between available traps. This idea was used by Reed [19] to derive a simple equation for the effective diffusion coefficient of helium in the presence of radiation induced vacancies The diffusion coefficient was given by

$$D^{\mathrm{He}} = \nu_{\mathrm{h}} \frac{\lambda^2}{6} C_{\mathrm{v}}^{-2/3} \exp\{-E_{\mathrm{He}}^{\mathrm{D}}/kT\} \qquad (1)$$

The definition and units of terms included in this equation and all subsequent equations are given in the nomencalture. A detailed study of helium migration in the presence of displacement damage is given in ref. [21b].

3. Dynamic re-solution of helium bubbles

Most of the existing fission gas behavior models for nuclear fuels recognize now the importance of the dynamic process by which fission fragments return the gas atoms to the matrix (for example see ref. [22]) In a fusion reactor structural material, bubble re-solutioning refers to the process by which helium gas atoms, present in bubbles in a metal lattice, are driven back into the matrix by irradiation. The importance of the radiation re-solution mechanism is widely accepted for the swelling of nuclear fuels [23]. In this section, we will establish a similar mechanism for helium bubbles in a structural material.

Two different re-solution mechanisms have been pre-

viously proposed in the literature for the treatment of the interaction between fission fragments and gas bubbles. The macroscopic model which was first proposed by Turnbull [24] depicts re-solutioning as the total destruction of every bubble contacted by an energetic fission fragment. Nelson [25], on the other hand, has proposed a microscopic model in which re-solutioning is assumed to occur by the interaction of the recoil atom flux and individual gas atoms Thus, the bubble is gradually dissipated by the loss of single gas atoms. In this section, we present an extension of Nelson's model to the calculation of the probability of re-solution in structural materials bombarded by neutrons

The re-solution parameter is the probability per second that a gas atom in a bubble receives an energy greater than the minimum energy, T_{min}, which a struck gas atom must acquire to be considered redissolved by a collision. This may occur directly by a neutron–helium gas atom collision or by recoil in an iron atom–helium gas atom collision. Schematically this can be shown as

$$(n) \rightarrow \left\{ \begin{matrix} \text{He gas} \\ \text{bubble} \end{matrix} \right\} \qquad (n) \rightarrow (Fe) \rightarrow \left\{ \begin{matrix} \text{He gas} \\ \text{bubble} \end{matrix} \right\}$$

direct collision — collision cascade generated by neutrons

The re-solution parameter for direct collisions [23] is

$$b_d = \int_{T_{min}/\Lambda_{He}}^{\infty} dE_n \, \Phi(E_n) \int_{T_{min}}^{\Lambda_{He} E_n} \times \sigma_{He-n}(E_n, T_d) \, dT_d \qquad (2)$$

and for collision cascades [23] it is

$$b_c = \int_{T_{min}/\Lambda}^{\Lambda_n E_n} dE_r \, \Phi(E_r) \int_{T_{min}}^{\Lambda' E_r} \times \sigma_{Fe-He}(E_r, T_r) \, dT_r. \qquad (3)$$

Stainless steel has a number of constituents. Because of the predominance of iron, a reasonable assumption is to consider the metal atoms in the lattice as iron The energy transfer parameter is given by $\Lambda = 4M_1M_2/(M_1 + M_2)^2$.

Since the values of the re-solution parameter, b, inferred from the experiments of Wapham [26] were at least an order of magnitude larger than those values calculated due to direct collisions, Nelson estimated b in nuclear fuels on the basis of colliions of gas atoms in the bubbles with a cascade of energetic secondary knock -ons. In a fusion neutron spectrum, however, the average neutron energy is quite high and the neutron can result in significant energy transfers to the light helium atoms. We will therefore consider re-solution by direct collisions as well as by collision cascades

3.1. Re-solution by direct neutron collisions

Assuming hard-sphere scattering, the elastic, isotropic scattering of neutrons on helium atoms is represented by the energy-transfer cross section. Substituting for $\sigma_{He-n}(E_n, T_d)$ in eq. (2) and integrating, yields

$$b_d \sim \sigma_s(n, He) \, \Phi(E_n). \qquad (4)$$

This result is applicable for a monoenergetic neutron flux, $\Phi(E_n)$, provided that $\Lambda_{He} E_n \gg T_{min}$. The direct collision re-solution parameter is thus independent of the gas density within the bubble and the minimum energy for re-solution. This implies that every direct collision of a neutron with a gas atom in the bubble will result in a re-solution event.

3.2. Re-solution by collision cascades

Recoil atoms and PKAs receive their energy from neutrons bombarding the metal lattice. The collision cascades created by PKAs passing near the bubble cause an energy transfer to the gas atoms, setting up a flux spectrum of recoil atom, $\phi(E_r)$. Consider the gas bubbles each containing m gas atoms immersed in a spatially uniform flux of recoil atoms. The recoil flux in the matrix is assumed to be the same as the recoil flux in the bas bubbles. To evaluate the re-solution probability per atom due to collision cascades, b_c, expressions for the recoil flux spectrum, $\phi(E_r)$, and the differential energy-transfer cross section between recoils and gas atoms, $\sigma_{Fe-He}(E_r, T_r)$, need to be derived.

For recoils with energies below about 100 keV the scattering cross section for collision with lattice or gas atoms can be approximated with that of hard spheres The angular cross section for hard-sphere scattering is isotropic in the center of mass system. Using the inverse potential function for the interaction between moving iron and helium atoms, the differential energy-transfer cross section can be shown as [27]

$$\sigma_{Fe-He}(E_r, T_r) = \frac{\sqrt{2}\,\pi \, Z_{Fe} Z_{He} a_B e^2 \exp(-1)(M_{He} + M_{Fe})}{\Lambda' \left(Z_{Fe}^{2/3} + Z_{He}^{2/3}\right)^{1/2} M_{He} E_r^2} = \frac{K}{E_r^2} \qquad (5)$$

The recoil flux spectrum, $\Phi(E_r)$, may be calculated by either solving the transport equation for the recoil ions or by using slowing down densities. Assuming hard-sphere scattering and a monoenergetic neutron

flux, results in the following expression for the recoil flux [27]

$$\phi(E_r) \approx \frac{2\phi\sigma_s(n,Fe)}{E_r^2\sigma_s(Fe,Fe)}\left(\Lambda_n\bar{E}_n - \frac{E_r^2}{\Lambda\bar{E}_n}\right) \quad (6)$$

where $\bar{E}_n$ is the average neutron energy.

The re-solution parameter can now be determined by inserting eqs. (5) and (6) into eq (3) and integrating. One finally obtains the following equation for the re-solution parameter for collision cascades:

$$b_c = BK\Phi\left[\frac{\Lambda'^3\Lambda_n\bar{E}_n}{6T_{min}^2} + \frac{\Lambda'}{\Lambda_n\bar{E}_n}\left(\ln\left(\frac{T_{min}}{\Lambda'}\right)+1\right) + \frac{\bar{E}_n}{\Lambda_n E_{n,max}^2}\left(\frac{T_{min}}{3\Lambda_n E_{n,max}} - \frac{\Lambda'}{2}\right) - \frac{1}{\Lambda_n\bar{E}_n}\left(\Lambda'\ln(\Lambda_n E_{n,max}) + \frac{T_{min}}{\Lambda_n E_{n,max}}\right)\right] s^{-1}, \quad (7)$$

where $B = 2\sigma_s(n, Fe)/\sigma_s(Fe, Fe) \simeq 4 \times 10^{15}\ \sigma_s(n, Fe)$. T_{min} is energy required to drive the struck helium atom through the gas in the bubble and implant it sufficiently deep in the solid so that it has little chance of migrating quickly back into the bubble. The value of T_{min} cannot be defined exactly, under the assumptions of the present model. We have neglected multiple gas collisions in the bubble, thereby resulting in no pressure dependence of the re-solution process. Also, how deep into the matrix must the gas atom be implanted such that it moves by random walk without correlation to the bubble location is dependent on T_{min}. A minimum energy, T_{min}, that is consistent with the present model is expected to be between the displacement threshold energy, E_d, and few hundred eV's.

In comparing the re-solution, parameter for a metal lattice with that derived for ceramic nuclear fuels, the value of b is concluded to be smaller for the metal lattice. This is consistent with the fact, as discussed by Nelson [25], that a fission fragment has a long track in comparison with the PKA range and causes intense ionization and lattice disturbance along its path. In metals the electron spike is dissipated very quickly by the free electron system and electrical neutrality is restored. Consequently, the positive ion cores do not have sufficient kinetic energy to cause a significant number of displacements. Excessive thermal vibrations give rise to a high temperature thermal spike along the range which has a lifetime typically of about 10^{-11} s. The high temperatures produce a significant thermal stress in the material causing the generation of a shock wave. There is speculation that the interaction of this shock front with a free surface can lead to atomic ejection in the form of plugs or chips of material [25]. This mechanism of "chips" was neglected, but may play a role, thereby increasing the value of the re-solution parameter. Possible improvements in the calculations include: (1) a better evaluation of the cross section $\sigma_s(Fe, Fe)$, (2) including the effects of energetic secondary knock-ons in the calculations of b_d, (3) more realistic interatomic potentials between helium and iron atoms, and (4) a more physical representation of T_{min}.

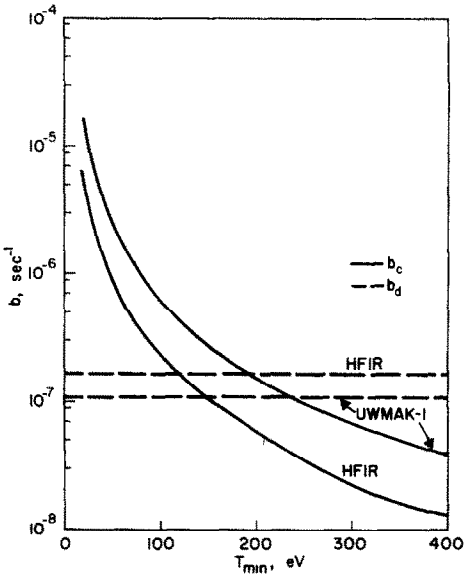

Fig 2 The microscopic re-solution parameter as a function of the minimum threshold energy for HFIR and UWMAK-I

Fig. 2 shows the results of the calculations of b_c and b_d for two reactors: HIFR and UWMAK-I[5]. HIFR has a higher neutron flux of lower average neutron energy. Since the flux is larger in HFIR than in UWMAK-I, the direct collision re-solution parameter is greater for HIFR. The converse is true for b_c because of the higher average neutron energy in UWMAK-I It will be shown that re-solution is an important factor determining low temperature swelling.

4. A simplified theory for helium swelling

4.1. Assumptions and equations

The detailed description of the interactions between point defects and helium generated by the (n, α) reac-

tion involves the solution of a large set of rate equations, one for each cluster size. Investigations using this approach [28,29] provide useful information on the basic mechanisms of interaction. The major difficulty is the excessive computational requirements. The model presented in this paper is much simpler. A qualitative description is given below.

Helium is assumed to migrate by an interstitial mechanism in between vacancy traps. Once two helium atoms collide, they form a di-helium gas atom cluster for which vacancies are readily available. Because of the possibilities of thermal dissociation and radiation resolution, this cluster is unstable. A tri-helium gas atom cluster is assumed to form the critical nucleus size for small gas-filled cavities. Nucleation is therefore dictated by the behavior of gas atoms rather than by vacancies. It has been recently discussed by Meyer et al. [30] that experimental evidence supports this assumption. The nucleation rate of cavities is the rate at which they cross this boundary in size space The density of cavities will therefore increase as the density of single and di-helium species increases. After a certain irradiation time, it becomes more probable for single helium to collide with larger size cavities than with the small nuclei Thus a gradual shift from the nucleation stage to the growth stage is achieved. The large size cavities are assumed to start growing from the nucleus size at only one average speed. The size distribution is therefore approximated by a delta function Keeping track of vacancy, interstitial and helium atom flows in and out of the average cavity determines its size and nature (void or bubble) at any time. Since interstitial loops nucleate rapidly during irradiation [28,29], their number density is assumed to be constant and they are only at a state of growth.

The physics covered by such a simplified description is obviously not exhaustive By order-of-magnitude comparison with the experiment, light can be shed on some possibly significant processes. The roles of vacancy loops, divacancies, precipitates, dislocation dynamics, cavity migration and coalescence, and matrix chemical changes in complex alloys are all neglected. Under these restrictive assumptions, the following rate equations describe swelling under conditions of simultaneous helium gas and displacement damage production.

$$\frac{dC_{He}}{dt} = P_{he} - 2K_{11}C_{He}^2 - K_{12}C_{He}C_{2He} - \bar{K}C_{He}N + 2(2C_{2He})\,b + mNb - Z_{He}^{d}\rho_d D^{He}C_{He} - 6D^{He}\frac{\sqrt{Z_{He}\rho_d}}{d}C_{He} + 2\gamma_h(2)\,C_{2He} \quad (8)$$

$$\frac{dC_{2He}}{dt} = K_{11}C_{He}^2 - K_{12}C_{he}C_{2He} - 2C_{2He}b + 3C_{3He}b - \gamma_h(2)\,C_{2He} \quad (9)$$

$$\frac{dC_{3He}}{dt} = K_{12}C_{He}C_{2He} - K_{13}C_{He}C_{3He} - 3C_{3He}b + 4C_{4He}b \quad (10)$$

$$\frac{dN}{dt} = K_{12}C_{He}C_{2He} - 3C_{3He}b \quad (11)$$

$$\frac{dC_v}{dt} = P_d - Z_v^{d}\rho_d D_v C_v - K_{vi}C_vC_i \quad (12)$$

$$\frac{dC_i}{dt} = P_d - Z_i^{d}\rho_d D_i C_i - K_{vi}C_vC_i \quad (13)$$

$$\frac{dm}{dt} = \frac{4\pi R_c D^{He}C_{He}}{\Omega} - bm \quad (14)$$

$$\frac{dR_c}{dt} = \frac{1}{R_c}\left\{D_vC_v - D_iC_i - D_vC_v^{e} \times \left[\exp\frac{\Omega}{kT}\left(\frac{2\gamma}{R_c} - p\right) - 1\right]\right\} \quad (15)$$

$$\frac{dR_{il}}{dt} = \frac{1}{b}\left\{Z_i^{d}D_iC_i - Z_v^{d}D_vC_v + D_vC_v^{e}\exp\frac{-(\gamma_{sf} + F_{el})\,b_v^2}{kT}\right\}, \quad (16)$$

where the concentrations are expressed in atoms per atom (apa) and the radii are in meters. The first three equations describe the concentrations of single gas atoms, C_{He}, diatomic clusters, C_{2He}, and triatomic clusters, C_{3He}. The fourth equation describes the total cavity number density, N.

The vacancy and interstitial concentrations, C_v and C_i, are represented by two coupled rates equations, eqs. (12) and (13). The last three equations describe the gas atom concentration in a cavity, m, the average radius R_c of the cavity, and the average interstitial loop radius, R_{il} [31].

The quantities K_{mn} are defined as follows:

$$K_{mn} = \frac{z_{mn}D^{He}}{a_0^2}. \quad (17)$$

The thermal dissociation parameter for di-gas atom clusters [32] is

$$\gamma_h(2) = \frac{D^{He}}{a_0^2}\exp\left(-\frac{E_{2He}^{B}}{kT}\right) \quad (18)$$

The elastic energy of a dislocation loop of radius R_{il} is

given by [31]

$$F_{el}=\frac{\mu b_v^2}{(1-\nu)\,4\pi(R_{il}+b_v)}\ln\left(\frac{R_{il}+b_v}{b_v}\right). \tag{19}$$

In eq. (10) it is assumed that $C_{4He}\approx C_{3He}$ in estimating the effects of re-solution. The equation for the nucleation rate of cavities (eq. 11) and the average number of gas atoms in a cavity (eq. 14) are derived by writing equations for the helium gas concentrations:

$$\frac{dC_{3He}}{dt}=K_{12}C_{He}C_{2He}-K_{13}C_{He}C_{3He}-3C_{3He}b+4C_{4He}b \tag{20}$$

$$\frac{dC_{4He}}{dt}=K_{13}C_{He}C_{2He}-K_{14}C_{He}C_{4He}-4C_{4He}b+5C_{5He}b \tag{21}$$

$$\frac{dC_{mHe}}{dt}=K_{1,m-1}C_{He}C_{(m-1)He}-K_{1m}C_{He}C_{mHe}-mC_{mHe}b+(m+1)\,C_{(m+1)He}b. \tag{22}$$

Since the number of gas atoms in a bubble nucleus is assumed to be three, the following approximations are made

$$K_{13}C_{He}C_{3He}+\cdots+K_{1m}C_{He}C_{mHe}\cong\bar{K}C_{He}N, \tag{23}$$

where $\bar{K}$ is an average reaction rate constant given by

$$\bar{K}=\frac{\sum_{j=3}^{m}K_{1j}C_{jHe}}{\sum_{j=3}^{m}C_{jHe}} \tag{24}$$

$$\frac{dN}{dt}=\frac{dC_{3He}}{dt}+\cdots+\frac{dC_{mHe}}{dt}=K_{12}C_{He}C_{2He}-3C_{3He}b-K_{1m}C_{He}C_{mHe}+(m+1)\,C_{(m+1)He}b\cong K_{12}C_{He}C_{2He}-3C_{3He}b. \tag{25}$$

Eq. (25) is particularly important during the nucleation phase where large size clusters have not formed. The last two terms are therefore neglected. The rate equation for the number of gas atoms in a cavity (eq. (14) is derived by following the model of Nelson [25], Pati [23], and Marlowe [34]. The model considers the growth of stationary bubbles by gas atom diffusion in the presence of radiation-induced re-solution. They assumed that the bubbles are small ($R\ll 10$ Å) and that the rate constants describing bubble growth are diffusion-controlled.

The rate equation for the interstitial loop radius, R_{il}, [31] is included in order to calculate the total dislocation density which changes with time due to a dependence on the fluence. The total dislocation density, ρ_d, is given by

$$\rho_d=\rho_d(0)+2\pi R_{il}N_{il}, \tag{26}$$

where the first term represents the initial network dislocation density and N_{il} is the interstitial loop density. Eq. (26) applies only where unfaulting of loops and network recovery are inoperable

4.2. Computational aspects

The previous set of interdependent non-linear ordinary differential equations constitute the core of the HEGBUF computer code It is a time-dependent program that was first implemented on the UCLA IBM System/370 model 3033. The GEAR computer package [35] is used to solve this system of equations The computer simulation is initialized by specifying the control options, input parameters, and the initial solution vector. Both continuous and interrupted-irradiations are simulated.

5. Correlation of the model with fission reactor data

The swelling model is mainly developed for applications to fusion conditions. Before we can achieve this objective, it is important to correlate with the existing HFIR swelling data. HFIR is deemed by some studies [3,36] to be suitable for material testing for fusion applications. A two-step nuclear reaction of nickel within stainless steel produces the largest amount of helium in high-flux reactors. The anticipated conditions of helium concentrations and displacement damage in a fusion reactor can easily be achieved by HFIR.

The input parameters are listed in table 1. The binding energy of di-helium atoms is assumed at 0.79 eV This corresponds to the value calculated for two helium atoms bound to one vacancy in Cu [37]. The cavity surface energy is fixed at 1000 erg/cm^2 [15]. A re-solution parameter of 10^{-6} s^{-1} is adopted in the calculations This corresponds to a minimum re-solution energy, $T_{min}\cong 40$ eV. It is to be noted that the re-solution parameter in nuclear fuels is in the range of 10^{-4} s^{-1} for a fission rate of $\sim 10^{13}$ fission/cm^3 [23]. Constant helium and damage generation rates of 6.025×10^{-11} at/at/s and 1.11×10^{-6} dpa/s are used in the calculations [36]. Using this set of input parameters, the results

Table 1
Material parameters for stainless steel

Parameter	Definition	Numerical value	Ref
a_0	lattice parameter	3 63 Å	[28]
k	Boltzmann's constant	$8\,617\times10^{-5}$ eV/K	
b_v	Burger's vector	2.5668×10^{-8} cm	[23]
z_{vi}	recombination combinatorial number	48	[23]
z_{11}	combinatorial number for He–He	84	[38]
z_{12}	combinatorial number for He–He_2	20	[38]
z_{13}	combinatorial number for He–He_3	12	[38]
d	grain diameter	3.0×10^{-3} cm	[16]
$\rho(0)$	initial value of dislocation density	10^8 cm/cm^3	
E^B_{2He}	binding energy of di-helium	0 79 eV	[37]
E^D_H	detrapping energy of helium	3.16 eV	[39]
E^F_i	formation energy of an interstitial	4.08 eV	[40]
E^M_i	migration energy of single interstitial	0 20 eV	[32]
E^F_v	formation energy of a vacancy	1 60 eV	[32]
E^M_v	migration energy of single vacancy	1 40 eV	[32]
γ	surface energy	$6\,24\times10^{14}$ eV/cm^2	[32]
Ω	atomic volume	1.1958×10^{-23} cm^3	[23]
ν	Poisson's ratio	0 291	[31]
$R_c(0)$	initial value of the cavity radius	5 Å	assumed
$R_{il}(0)$	initial value of the interstitial loop radius	5 Å	assumed
γ_{sf}	stacking fault energy	9.2×10^{12} eV/cm^2	[31]
μ	shear modulus	1.7665×10^{23} eV/cm^3	[31]
B	Van der Waals' constant	1.75×10^{-23}	[43]
ν_H	helium vibrational frequency	$5\,0\times10^{14}$/s	[44]
ν_i	interstitial vibrational frequency	$5\,0\times10^{12}$/s	[45]
ν_v	vacancy vibrational frequency	5.0×10^{13}/s	[43]
Z_{He}	bias factor of helium gas atoms	1.00	
Z_i	bias factor of interstitials	1 08	[31]
Z_v	bias factor of vacancies	1.00	

of the calculations will be analyzed and compared to the experimental data in this section.

The temporal concentrations of single, di-helium and cavity number densities are plotted in figs. 3 and 4 for 753 K and 953 K, respectively. At both temperatures the helium concentration is observed to increase in an approximately linear manner at the start of irradiation as helium is being produced. After a period of time, the loss rates of helium become significant and the concentrations of single helium atoms and small helium clusters begin to level off and then decline. The cavity number density, on the other hand, increases monotonically as a function of time. However, the nucleation current decreases as the chances for growth increase We will use here a convenient definition of the nucleation time as the time beyond which growth of existing cavities is more probable than nucleation of new ones. In order to quantify this definition, we calculate the relative probability of growth as the ratio of the growth rate divided by the sum of both the nucleation and growth rates. When this probability reaches $(1-e^{-1})$, nucleation is practically non-existent. This time is $\sim 2\times10^6$ s at 753 k, while it is ~ 5000 s at 953 K. The effect of bubble re-solutioning is also shown in figs. 3 and 4. At the lower temperature (753 K), re-solutioning results in a higher single gas atom concentration and a lower cavity number density. The dynamic collisions between neutrons and helium atoms in bubbles or the collision cascades by the neutrons coupled with the low diffusion rates of helium increase the single helium concentration and reduce the concentration of cavities At the higher temperature the situation is not as straightforward. The higher single gas atom concentrations due to re-solutioning generally promote bubble nucleation, and

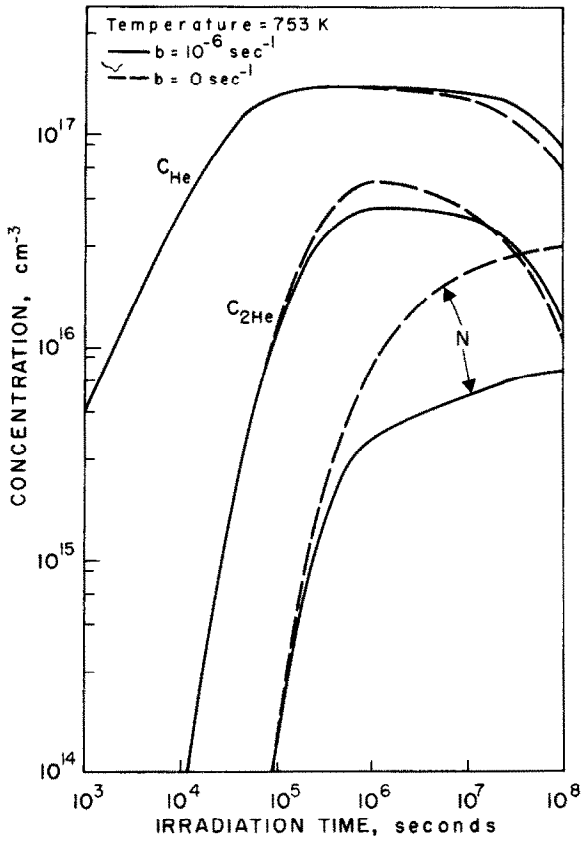

Fig 3 Helium cluster concentrations at 753 K for HFIR

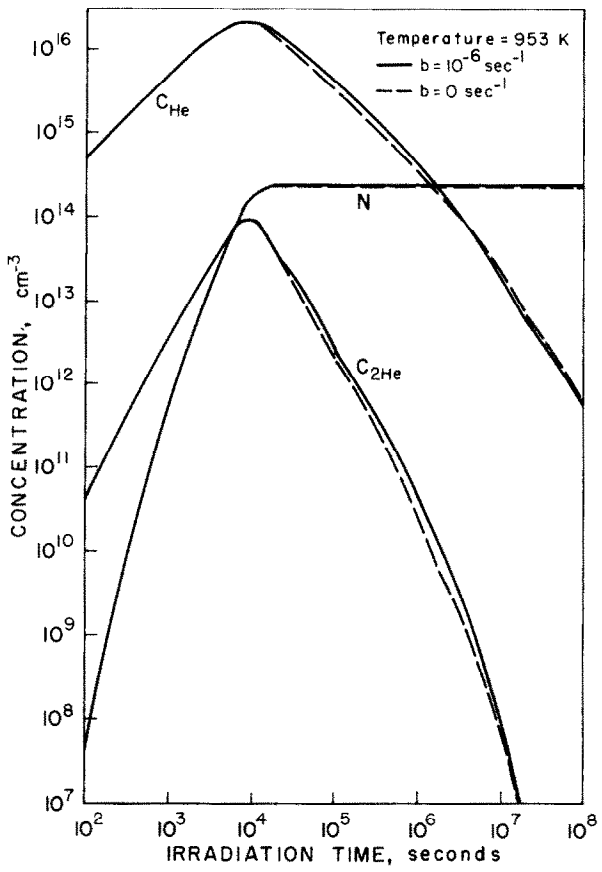

Fig 4 Helium cluster concentrations at 953 K for HFIR

the cavity number density increases slightly due to re-solutioning

The nature of the average gas-filled cavity is expressed in terms of the surface tension force, $2\gamma/R_c$, and the internal helium gas pressure, P_g. Mechanical equilibrium is achieved when $P_g = 2\gamma/R_c$. The set of curves plotted in fig. 5 show the two parameters as functions of the irradiation time. The cavities are not in mechanical equilibrium except at the highest temperature, and only for a few thousand seconds.

Comparisons between the model predictions and HFIR data are shown in figs. 6 and 7. The average cavity radius remains at approximately the initial value until $\sim 10^4$ s The radius starts to increase rapidly after this slow growth period. The average radii predicted by the model are roughly within the experimental results of HFIR. It is emphasized here that such a close agreement does not mean that the theory is all encompassing. Additional physics have to be included as new data become available. The swelling results are shown in fig 7. Notice the importance of gas re-solutioning where the swelling is extremely high at the lower temperatures if $b = 0$ The increase in the swelling with decreasing temperatures is due to the increase in the cavity density. Whereas EBR-II swelling data shows a peak around 500°C, the swelling peak here appears to be at a much lower temperature. This is in qualitative agreement with recent HFIR data [42]. The transient swelling results of high He/dpa (HFIR) and low He/dpa (EBR-II) facilities seem to be different.

6. Applications to fusion reactors

Due to the wide variation in the operational characteristics of conceptual MCFR's, we will proceed in this section by analyzing the results for three representative fusion reactors. In this section, the model is applied

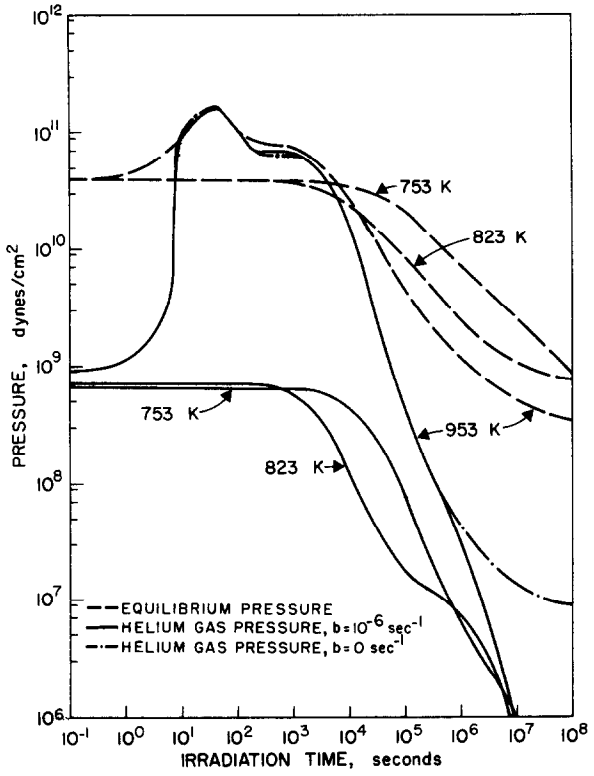

Fig. 5 Time-dependent helium and equilibrium pressures in the average HFIR cavity

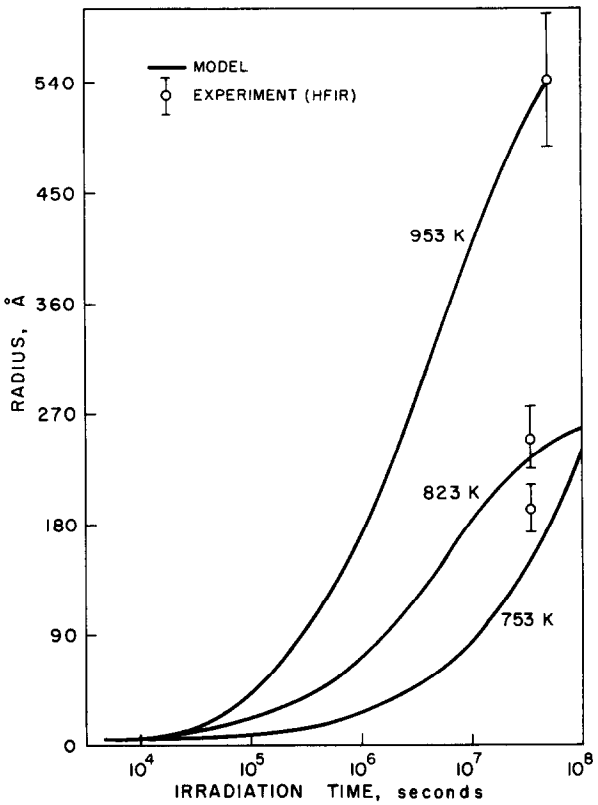

Fig. 6. Comparison between the calculations of the average cavity size in 316 stainless steel and HFIR experimental data

to the irradiation conditions of the Wisconsin tokamak conceptual design UWMAK-I [5], the International Tokamak Reactor INTOR [6], and the UCLA DD Tandem Mirror SATYR [47]. Relevant input parameters of these reactors are listed in table 2. Calculations for continuous as well as pulsed irradiations are performed for the UWMAK-I and INTOR reactors. Radiation pulsing is simulated by setting the displacement damage rate, helium production rate and the re-solution parameter to their respective values during the on-time and to zero during the off-time.

6.1. *The Wisconsin Tokamak Reactor UWMAK-I [5]*

UWMAK-I is a D–T fusion reactor based on the Tokamak confinement concept. The neutron wall loading on the first wall is 1.25 MW/m^2. The total flux in the first centimeter of the first wall is about 4.757×10^{14}

Table 2
Input parameters for the three fusion concepts

Reactors	Time (s)			Re-solution parameter (s^{-1})	Damage rate (dpa/yr)	Helium production (appm/yr)
	Burn	Off	Cycle			
UWMAK-I [5]	5400	390	5790	10^{-5}	18 2	298
INTOR [6]	75	25	100	10^{-5}	23 3	294
SATYR [45] front zone (0–1 cm)	Steady irradiation			10^{-7}	6 93	53 58

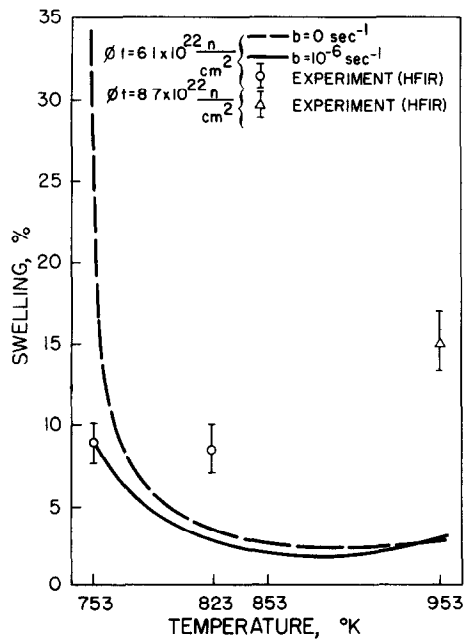

Fig 7 Comparison between the calculations of the percent swelling in 316 stainless steel and HFIR experimental data

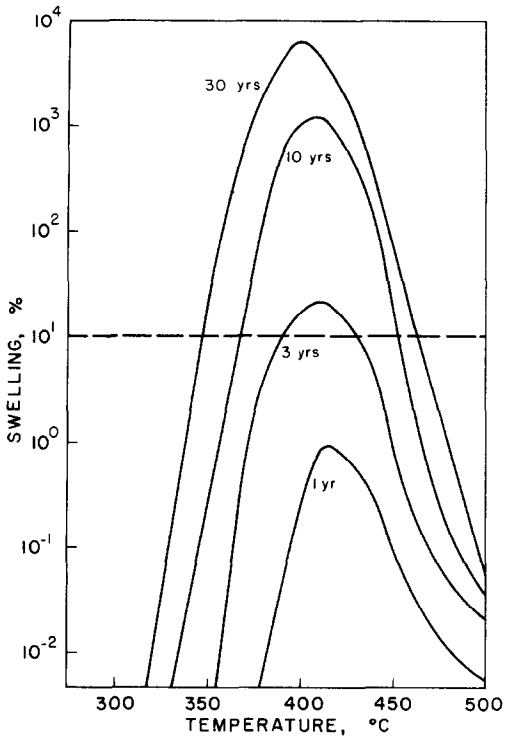

Fig 8 Swelling as a function of temperature in UWMAK-I after various periods of continuous irradiation

$n/cm^2 \cdot s$ and the average neutron energy is about 4 18 MeV. The re-solution parameter is therefore set to 10^{-5} s^{-1} which corresponds to a minimum threshold energy of 20 eV, as analyzed in section 3.

The swelling curves for continuous irradiations are shown in fig. 8. Maximum swelling occurs around 400°C The swelling curve in UWMAK-I predicted by the University of Wisconsin Fusion Feasibility Group [5] at 2.5×10^{23} n/cm^2 and 118 dpa ($\simeq 6$ yr) shows a peak in the swelling at 500°C of about 118%. They based their prediction on the neutron irradiation data and heavy ion simulation studies. Swelling values greater than 5–10% can not be tolerated without major design modifications. The lifetime of this first wall will probably be longer than 3 years if the irradiation temperature is greater than 450°C

The effects of long burn-time pulsing on the previous results are studied by analyzing the damage and helium dynamics for nine consecutive pulses. Fig. 9 shows the concentrations of single helium atoms, di-helium clusters, and cavities for nine pulses. The concentrations increase almost linearly during the first on-time. During the shutdown periods of the reactor, the concentration of single helium atoms is rapidly depleted by the formation of larger size clusters. As can be seen from the figure, this gives rise to a fast increase in the concentration of di-helium cluster atoms which, by interaction with single helium atoms, leads to an increase in the cavity number density It is interesting to note that the cavity number density increases during the shutdown periods of the reactor and stays essentially at a dynamic equilibrium during the burn-time. This effect is similar to Ostwald ripening in solid state reactions. The gradual increase in the vacancy concentration during each on-time, and the depletion of matrix vacancies during the off-time result in an overall higher helium mobility for pulsed irradiations. This generally leads to a faster clustering rate, and an early saturation of the cavity concentration because part of the helium is lost to dislocations. Pulsing can therefore be viewed as an effective increase in the irradiation temperature

The average cavity radius is shown in fig 10 as a function of irradiation time. The radius increases mainly during the on-time The growth rate of cavities is slightly smaller during pulsed irradiation due to a higher rate of point defect recombination. The net result is a smaller cavity radius for the pulsed case. After nine pulses, the radius is about 0.01 Å smaller than the corresponding continuous irradiation value. This is perhaps a small

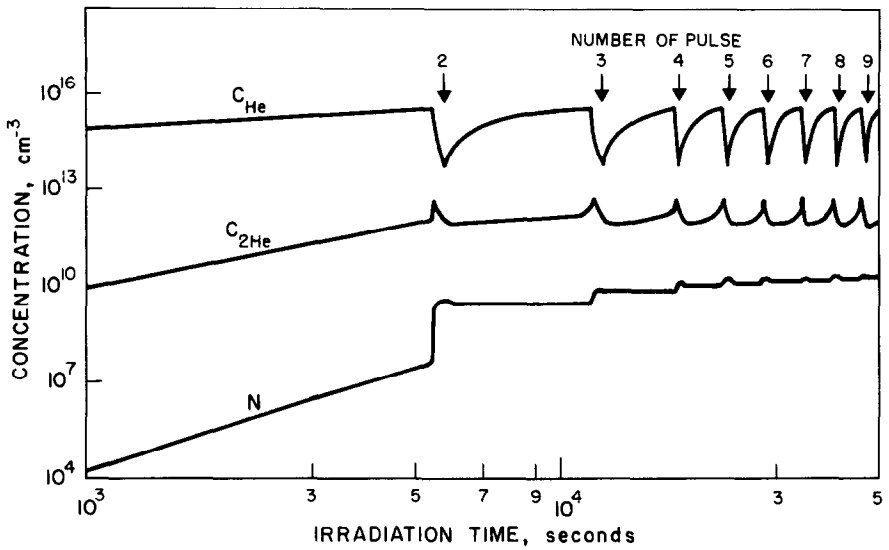

Fig 9 Pulsed helium cluster concentrations in UWMAK-I at 500°C

value, but over thousands of pulses the overall effect is great. Continuous irradiation calculations may therefore give a conservative estimate of the anticipated swelling in pulsed fusion reactors.

6.2. *The international Tokamak Reactor (INTOR)* [6]

The first wall material of the International Tokamak Reactor (INTOR) is chosen as 316 stainless steel, even though other materials are considered. The neutron wall loading is about 1.3 MW/m^2. The maximum structural temperature is determined to be less than 400°C.

The time-dependent swelling values at 500°C for both INTOR and HFIR are shown in fig. 11. The calculations here are performed for equivalent continuous irradiation under INTOR conditions where the damage was averaged over both on-and off-times. Due to the lower displacement damage and helium production rates in INTOR, swelling is at least an order of magnitude lower than HFIR.

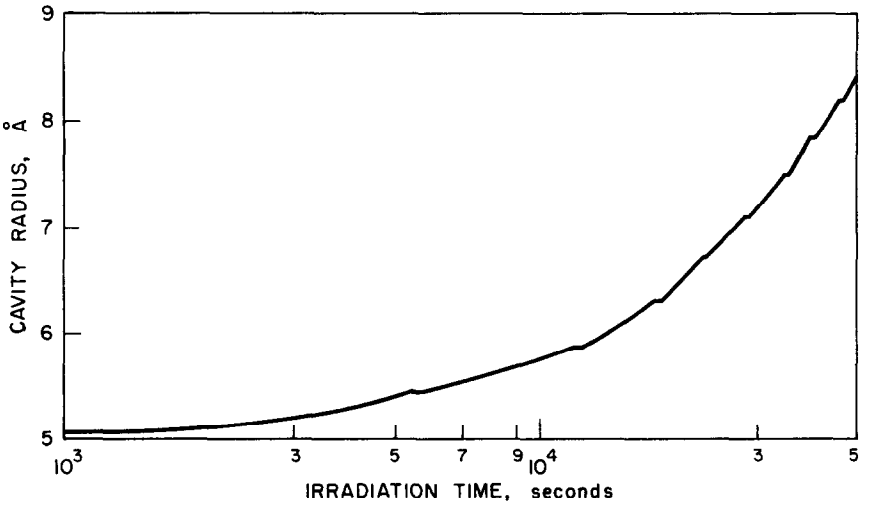

Fig 10 Average cavity radius as a function of irradiation time for nine consecutive pulses in UWMAK-I at 500°C

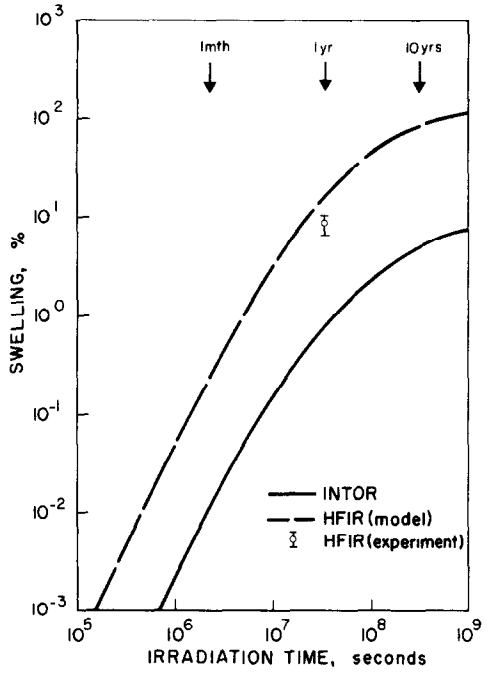

Fig 11 Comparison between the percent swelling in HFIR and INTOR.

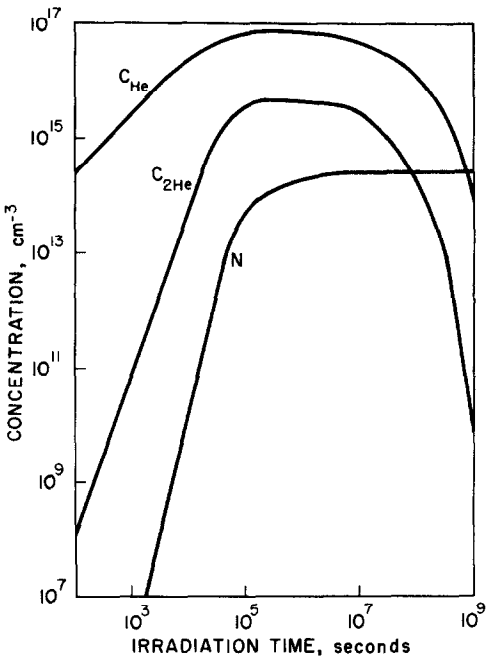

Fig 12 Helium cluster concentrations as functions of irradiation time for INTOR at 500°C

The temporal concentrations of single helium atoms, di-helium clusters and larger cavities are plotted in fig. 12 at 500°C. While the single and di-helium concentrations decline after ~ 15 days, the cavity number density remains at its saturation value. The growth of the cavity and loop microstructure reduces the single vacancy concentration. The mobility of helium is therefore increased and a decline in the concentration of single helium atoms is observed. Consequently, the formation rate of di-helium clusters decreases and cavity nucleation terminates. The diffusion coefficient of helium is $\sim 4.8 \times 10^{-17}$ cm^2/s between 10^4 to 10^7 s, and rises to 3.5×10^{-16} cm^2/s by 10^9 s.

The effects of relatively rapid pulsing are shown in fig. 13, where the behavior of single helium atoms and helium clusters during the first 100 pulses is shown. The on-time is 75 s and the off-time is 25 s. The cavity formation is observed to be faster during the initial stages (first 60 pulses) of irradiation in the pulsed case when compared to equivalent continuous irradiation. The higher effective helium diffusivity in the pulsed case results in a rapid saturation of the single helium concentration and a corresponding higher bubble density. During the later stages of irradiation, however, the continuous irradiation results show an increase in the number density while the increase is much smaller in the pulsed case. Notice here that the displacement damage and helium production rates are modified in the continuous irradiation case to produce the same *average* values as in the corresponding pulsed irradiation. It is also to be noted that the total helium in clusters is *not*

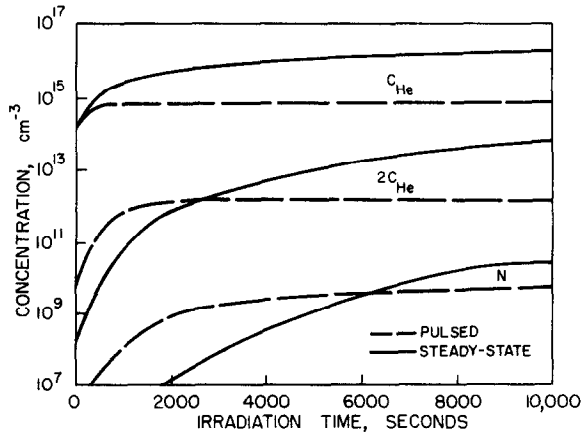

Fig 13 Comparison between helium cluster concentrations for pulsed and continuous irradiations in INTOR at 500°C

conserved between the two cases because dislocations are assumed to trap a fraction of the mobile helium. This fraction is greater in pulsed irradiation because of the effective higher mobility.

6.3. The UCLA DD-Tandem Mirror SATYR [47]

In fusion reactors based on the D–D fuel cycle, the plasma power density is lower than the corresponding D–T fusion cycle. A consequence of the low plasma power density is a reduced neutronic wall loading. The UCLA DD-Tandem Mirror is essentially a steady-state machine designed with a neutron wall loading of ~ 0.4 MW/m^2. The first wall thickness is 2.2 cm giving a total neutron flux variation of 3.45×10^{14} n/cm$^2 \cdot$ s in the front zone down to 2.37×10^{14} n/cm$^2 \cdot$ s at the back end of the first wall. The spatial flux and neutron spectral variations in the first wall are found to have drastic effects on cavity formation. For example, the cavity density drops by roughly an order of magnitude between the front and back zones of the first wall at 500°C. Fig. 14 shows the total cavity concentration as a function or irradiation time at different temperatures. It is observed that the higher helium mobilities at high temperatures lead to an early saturation of the cavity concentration. Both the nucleation time (approximately the time to saturation) and the saturation cavity density decrease as a function of increasing temperature. This is qualitatively consistent with experimental findings.

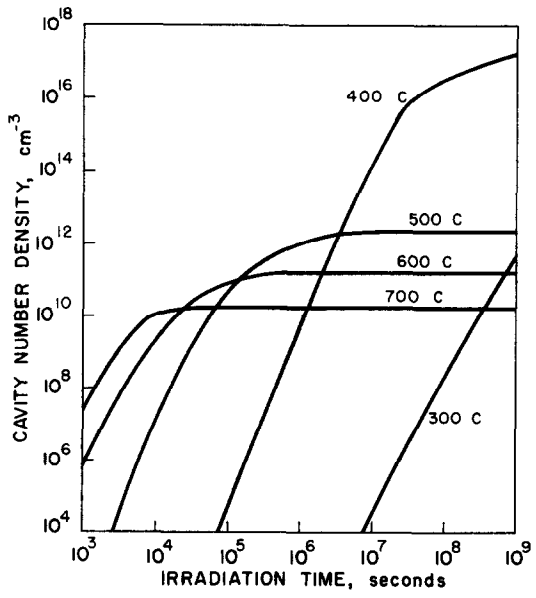

Fig 14 Dependence of the cavity number density on irradiation time for the SATYR DD Tandem Mirror

7. Conclusions

The theoretical model presented here for the time-dependent behavior of intragranular helium gas is primarily applicable to fusion reactor conditions where helium gas is assumed to dictate the nucleation of small vacancy-helium clusters. Helium is assumed to be simply migrating interstitially in between vacancy traps. The mobility of helium, therefore, decreases as irradiation increases the concentration of those traps. During radiation pulsing, an interesting scenario occurs. Vacancy traps increase during the on-time and gradually immobilize helium reducing the nucleation rate of cavities. When the pulsed source if turned off, matrix vacancies are depleted by migration to internal sinks. Helium is therefore made highly mobile again during the off-time giving rise to an increase in the nucleation rate of small size helium-vacancy clusters. The overall result of this behavior is a higher effective helium mobility during pulsed irradiation. One way of interpreting this behavior is to simply regard it as equivalent to an increase in the irradiation temperature. Recent experiments by Packan [46] suggest a similar interpretation.

Although we have treated small helium-vacancy clusters in some detail, the model is not exhaustive. The role of small mobile clusters such as di-vacancies containing a substitutional helium atom was not assessed. The model gives reasonable correlation with the existing HFIR data. A more expanded theoretical treatment that is based on a wider data base may be necessary to identify other important processes relating to the synergistic interaction between helium and displacement damage. The following conclusions are drawn from this work:

(1) The nucleation and growth phases of helium-filled cavities are simultaneously treated.

(2) The dynamic dispersion of helium atoms into the matrix by radiation (re-solutioning) is recognized to be an important process especially at low temperatures.

(3) Thermal dissociation of di-helium atom clusters is important only at high temperatures ($\gtrsim$ 600°C).

(4) Order-of-magnitude agreement between the model and HFIR swelling data is achieved over a limited temperature range (480–680°C).

(5) Assuming a 10% swelling design limit and a lifetime expectancy of 10 years for the fusion reactor first wall, the blanket temperature must be kept roughly below ~ 350°C or above ~ 500°C for the 3 design

concepts considered in this study.

(6) Radiation pulsing tends to decrease the average cavity radius and number density, which results in the suppression of swelling, however, bubble coalescence and vacancy loop evaporation during the off-time, which are not included in the theory, may counteract this result.

(7) Cavities are generally non-equilibrium bubbles due to re-solutioning. The gas pressure is less than the surface tension force except for high temperatures ($\gtrsim$ 600°C).

Acknowledgements

The financial support of the National Science Foundation through grant number ENG-78-05413 is greatly acknowledged. The valuable input of the Radiation Effects group of ORNL is especially appreciated.

Nomenclature

Symbol	*Definition*	*Units*
a_B	Bohr radius	m
a_0	Lattice parameter	m
$b = b_c + b_d$	Total re-solution parameter	s^{-1}
b_c	Probability of re-solution of a single gas atom by a collision cascade per second	s^{-1}
b_d	Probability of re-solution of a single gas atom by a direct neutron collision per second	s^{-1}
b_v	Burger's vector	m
$C_{v,i}$	Vacancy/interstitial concentration	at/at
$C_{n\mathrm{He}}$	Concentration of size n helium cluster	at/at
C_v^e	Thermal equilibrium vacancy concentration	at/at
d	Grain diameter	m
D^{He}	Helium effective diffusion coefficient	m^2/s
$D_{v,i}$	Vacancy/Interstitial diffusion coefficient	$m^2\ s^{-1}$
e	Electronic charge	Coulomb
E_{He}^D	Helium detrapping energy	J
E_r	Recoil atom energy	J
$\bar{E}_n$	Average neutron energy	J
E_n	Neutron energy	J
$E_{n,\max}$	Maximum neutron energy	J
$E_{2\mathrm{He}}^B$	Binding energy for di-helium clusters	J
F_{el}	Dislocation loop line tension	J/m^2
k	Boltzmann's constant	J/K
K_{vi}	Recombination rate constant	s^{-1}
K_{nm}	Rate constant for the interaction of size n and size m helium clusters	s^{-1}
$\bar{K}$	Average reaction rate constant	s^{-1}
m	Number of helium atoms in an average size cavity	—
$M_{\mathrm{He,Fe}}$	Atomic masses of He and Fe	a.m.u.
N	Total concentration of helium-vacancy clusters	at/at
P_d	Displacement damage production rate	at/at/s
P_g	Gas pressurre in the average cavity	N/m^2
P_{He}	Production rate of helium gas atoms	at/at/s
R_c	Average cavity radius	m

Symbol	Definition	Units
R_{il}	Average interstitial loop radius	m
T	Irradiation temperature	K
T_d	Threshold displacement energy	J
T_{min}	Minimum energy required for helium re-solution	J
z_{nm}	Size dependent combinatorial number for n and m helium clusters	–
$Z_{He,Fe}$	Charge numbers for He and Fe	–
Z^d_{He}	Bias factor of dislocations toward helium	–
$Z^d_{v,i}$	Dislocation bias factors for vacancies/interstitials	–
γ_{sf}	Stacking fault energy	J/m^2
$\gamma_h(2)$	Thermal dissociation rate of di-helium clusters	s^{-1}
Λ'	Energy transfer parameter for an Fe–He collision	–
Λ_{He}	Energy transfer parameter in a hard-sphere scattering between a neutron and a helium atom	–
λ	Interatomic jump distance	m
ν	Poisson's ratio	–
ν_h	Helium vibrational frequency	s^{-1}
μ	Shear modulus	J/m^3
Ω	Atomic volume	m^3
Φ	Neutron or recoil flux	$m^{-2}\,s^{-1}$
ρ_d	Network dislocation density	m^{-2}
$\sigma_{He-n}(E_n, T_d)$	Differential elastic scattering cross section for a neutron of energy E_n and helium recoil of energy T_d	m^2J^{-1}
$\sigma_{Fe-He}(E_r, T_r)$	Differential elastic scattering cross section for an iron atom of energy E_r and a helium recoil of energy T_r	m^2J^{-1}
σ_s(n, He)	Microscopic elastic scattering cross section for n–He interaction	m^2
σ_s(n, Fe)	Microscopic elastic scattering cross section for n–Fe interaction	m^2
σ_s(Fe, Fe)	Microscopic elastic scattering cross section for Fe–Fe interaction	m^2

References

[1] D.N. Braski, J. Schroeder and H. Ullmaier, J. Nucl Mater. 83 (1979) 265.

[2] P. Maziasz and M.Z. Grossbeck, Proc. 2nd Topical Meeting on Fusion Reactor Materials, Seattle, WA, 1981.

[3] G.L Kulcinski, D.G. Doran, and M. Abdou, ASTM-STP-570 (Amer. Soc. for Testing and Materials, Philadelphia, PA, 1975) p. 329.

[4] R.G. Mills, A Fusion Power Plant (Princeton University, MATT-1050, 1974) p. 292.

[5] B. Badger et al., UWMAK-I, Univ. of Wiscons. in Report, UWFDM-68, Vol I (1973).

[6] International Tokamak Reactor Zero Phase, R.S. Pease, Chairman, IAEA Vienna (Unipub, New York, 1980) p. 384.

[7] G.R. Odette and S C. Langley, Radiation Effects and Tritium Technology for Fusion Reactors, Eds. J.S. Watson and F.W. Wiffen, Vol. I, CONF-750989 Nat. Tech. Inf. Service, Springfield, VA, 1976 p. 395

[8] F.V Nolfi, Jr., A. Taylor, D I. Potter, S.C. Agarwal and B. Okray Hall, Trans. Am. Nucl. Soc. 26 (1970) 190.

[9] F.V. Nolfi, Jr and Che-Yu Li, Nucl. Technol. 38 (1978) 405.

[10] K. Farrell, M.B. Lewis and N.H. Packan, Scripta Metall. 12 (1977) 1121.

[11] W.J Choyke, J.N. McGruer, J.R. Townsend, J.A. Spitznagel, N.J Coyle and F.J. Venskytis, Helium Effects in Ion Bombarded 304 Stainless Steel (Univ. of Pittsburgh and Westinghouse Research and Development Center, preprint 1979).

[12] F W. Wiffen and E.E. Bloom, Nucl. Technol 25 (1975) 113.

[13] B. Okray Hall, J. Nucl. Mater. 85 (1979) 565.
[14] G. Odette and M. Frei, Proc. 1st Topical Meeting on Technol. of Controlled Nuclear Fusion, Eds. G.R Hopkins and B. Yalof, Vol. II, CONF-740402-P2 (Amer Nucl. Soc., San Diego, CA, 1974) p. 485
[15] S E. Maydet and K C. Russell, J Nucl. Mater 82 (1979) 271.
[16] Che-Yu Li, J. Rest, S. Danyluk and R.B. Peoppel, Proc. 2nd Topical Meeting on the Technolgy of Controlled Nuclear Fusion, Ed. G.L. Kulcinski, CONF-760935-PI (Energy and Research Development Administration, Washington, DC, 1976) p 239.
[17] R.W. Conn, in: Fusion, Ed. E. Teller (Academic Press, New York, 1980).
[18] W.D. Wilson and C.L. Bisson, Phys Rev B1 (1970) 3510.
[19] R.J. Reed, Radiat. Eff. 31 (1977) 129.
[20] F.A. Smidt, Jr and A.G. Pieper, ASTM STP 570 (Amer. Soc. for Testing and Materials, Philadelphia, PA, 1975) p. 352
[21] (a) V. Philipps, K. Sonnenberg and J.M. Williams, Consultants Symposium on Rare Gases in Metals and Ionic Solids, 1979, AERE Harwell, England
(b) N.M. Ghoniem and S. Sharafat, Proc Yamada Conf. on Point Defects, Kyoto, Japan, 1981
[22] J.M. Griesmeyer, N.M. Ghoniem and D. Okrent, Nucl. Eng. Design, 55 (1979) 69
[23] D.R. Olander, Fundamental Aspects of Nuclear Reactor Fuel Elements, TID-26711-P1 (NTIS, Springfield, VA, 1976).
[24] J.A. Turnbull, J. Nucl. Mater. 38 (1971) 203
[25] R.W. Nelson, J. Nucl. Mater. 31 (1969) 153.
[26] A.R. Whapham, Nucl. Appl. 2 (1966) 123.
[27] M.L. Takata and N.M. Ghoniem, Plasma Physics and Fusion Engineering Report, UCLA, PPG-519 (1980).
[28] M.R Hayns, J. Nucl. Mater. 59 (1976) 195.
[29] N.M Ghoniem and D.D. Cho, Phys Status Solidi 54 (1979) 171.
[30] R.M Mayer, J Nucl. Mater. 95 (1980) 83
[31] N.M. Ghoniem and G.L. Kulcinski, Radiat. Eff. 39 (1978) 47
[32] D.D. Cho and N.M. Ghoniem, The Initial Stages of Point Defect Clustering in Fusion Reactor First Wall (Univ of Calif., Los Angeles, UCLA-ENG-7935, 1979)
[33] S.R. Pati, Trans. Am. Nucl. Soc 14 (1971) 580
[34] M.O. Marlowe, General Electric Company, USAEC Report GEAP-12148, 1970.
[35] A.C. Hindmarsh, LLL Report, UCID-30001, Rev. 3, 1974
[36] P.J Maziasz, F.W Wiffen and E.E Bloom, Radiation Effects and Tritium Technol. for Fusion Reactors, Eds J.S. Watson and F.W. Wiffen, Vol. I, CONF-750989 (NTIS, Springfield, VA, 1976) p 259.
[37] W.D. Wilson, M.I. Baskes and C.L. Bisson, Phys Rev., B13 (1976) 2474.
[38] M deJong and J.S. Koehler, Phys. Rev 129 (1963) 40
[39] W.D. Wilson and R.A. Johnson, Interatomic Potentials and Simulation of Lattice Defects, Eds. C Gehlen, J R Beeler and R I. Jaffree (Plenum Press, New York, 1972) p. 375.
[40] R.A. Johnson, Phys. Rev. 145 (1966) 423
[41] N.V Tsederberg, V.N Poper and N.A. Morozona, Thermodynamic and Thermophysical Properties of Helium, transl. TT 70-50096 (Nat Techn. Inf. Service, Springfield, VA, 1971).
[42] B Okray Hall and H Wiedersich, J Nucl Mater 66 (1977) 187
[43] R A. Johnson, J Nucl. Mater 75 (1978) 77
[44] P J Maziasz, unpublished work, private communications
[45] N M Ghoniem and R W Conn, Proc IAEA Technical Committee Meeting, Tokyo, Japan, Oct 1981
[46] B Badger et al, Univ of Wisconsin Fusion Report, UWFDM-330 (1979)